

# Evolution of Thick Accretion Disks Produced by Tidal Disruption Events

Andrew Ulmer<sup>1</sup>

Princeton University Observatory, Peyton Hall, Princeton, NJ 08544

submitted to *ApJ*, August 1997

## ABSTRACT

Geometrically thick disks may form after tidal disruption events, and rapid accretion may lead to short flares followed by long-term, lower-level emission. Using a novel accretion disk code which relies primarily on global conservation laws and the assumption that viscosity is everywhere positive, a broad range of physically allowed evolutionary sequences of thick disks is investigated. The main result is that accretion in the thick disk phase can consume only a fraction of the initial disk material before the disk cools and becomes thin. This fraction is  $\sim 0.5 - 0.9$  for disruptions around  $10^6$  to  $10^7 M_\odot$  black holes and is sensitive to the mean angular momentum of the disk. The residual material will accrete in some form of thin disk over a longer period of time. The initial thick disk phase may reduce the dimming timescale of the disk by a factor of  $\sim 2$  from estimates based on thin disks alone. Assuming an  $0.5 M_\odot$  initial thick disk, even if the thin disks become advection dominated, the black hole mass to light ratio can rise above  $M_\odot/L_\odot = 1$  in no less than 20 ( $0.1/\alpha$ ) to 2000 ( $0.1/\alpha$ ) years following a tidal disruption event, depending on the mass of the black hole and the initial conditions of the encounter. The long-term emission will be most prevalent around lower mass,  $10^6 M_\odot$  black holes. If the tidal disruption rates in these galactic nuclei are  $\sim 10^{-4} \text{ yr}^{-1}$ , then about 10% of the nuclei should exhibit the long-term UV/optical emission at a level of  $\sim 10^{38} \text{ ergs s}^{-1}$ .

*Subject headings:* accretion, accretion disks – black hole physics – galaxies: nuclei – quasars: general

---

<sup>1</sup>andrew@astro.princeton.edu

## 1. Introduction

If black holes reside in the centers of galaxies, one clinching sign of their existence would be the tidal disruption of stars when a star passes within a tidal radius,  $R_t \sim 25M_6^{-2/3}R_S$ , of the black hole, where  $M_6$  is the black hole mass in units of  $10^6M_\odot$  and  $R_S$  is the Schwarzschild radius. Tidal disruption events are rare ( $\sim 10^{-4}$  per year per  $L_\star$  galaxy), bright ( $L \sim L_{\text{Edd}}$ ), short (months to years), and seemingly unavoidable consequences of  $10^6 - 10^8M_\odot$  black holes in galactic centers. The general picture for tidal disruption of a star has been developed over the last 20 years (e.g. Hills 1975; Young, Shields, & Wheeler 1977; Rees 1988). The picture has evolved from one in which the disruption rate was so high as to fuel quasars to one with a more modest rate in which disruptions are rare transients which may nevertheless, slowly grow a lower mass,  $\sim 10^7M_\odot$ , black hole (Goodman & Lee 1989).

At the time of disruption, half of the star is captured onto a range of elliptical orbits around the black hole; the remainder is ejected from the system. Due to the relativistic effect of orbital precession, debris orbits cross and may form strong shocks (Rees 1988). The explicit evolution of the debris is complex and is dependent on the spin and mass of the black hole as well as the properties of the star and the stellar orbit. As discussed by Kochanek (1994), at intersections between the debris streams, energy and angular momentum may be transferred. The computational complexities of the problem prohibit a direct numerical solution, but as an approximation, a large fraction of the debris can be said to circularize in a time,

$$t_{\text{cir}} = n_{\text{orb}}t_{\text{min}}, \quad (1)$$

where  $n_{\text{orb}}$  is a number greater than 1, and probably between 2 and 10. The minimum return time,  $t_{\text{min}}$  is the time for the most bound material to return to pericenter,  $R_p$  is

$$t_{\text{min}} = \frac{2\pi R_p^3}{(GM_{\text{BH}})^{1/2}(2R_\star)^{3/2}} \approx 0.11 \left(\frac{R_p}{R_t}\right)^3 \left(\frac{R_\star}{R_\odot}\right)^{3/2} \left(\frac{M_\star}{M_\odot}\right)^{-1} M_6^{1/2} \text{years}, \quad (2)$$

where  $R_\star$  and  $M_\star$  are the radius and mass of the disrupted star.

The circularization process may produce a thick torus which would accrete on a fast timescale. Initially, the disk is expected to be geometrically thick and radiation pressure supported, because of the large energy difference ( $\sim GMM_\star/8R_p$ ) between the nearly unbound elliptical orbits and a subsequent circular orbit at  $\sim 2R_p$ , which is set by conservation of angular momentum. The disk is also highly optically thick with  $\tau > 10^6$ . In comparison, our sun has  $\tau \sim 10^{11}$  and a radius  $\sim 100$  times smaller than the characteristic radius of a thick disk. The thick disk's structure is very much like the envelopes of massive stars, except that self gravity plays no role; the gravity in the disks is dominated

by the black hole. The disk will remain geometrically thick if energy is dissipated fast enough. In general, this energy dissipation rate corresponds to an accretion rate which is super-Eddington. The physical parameters of an tidal disruption encounter which produce super-Eddington accretion are described in Ulmer (1997; hereafter U97). Delineating the region in which thick accretion occurs is important not only because super-Eddington tidal disruption events are the brightest and therefore, the most readily observed flares, but also because one expects the accretion of the stellar debris to be fastest when the disk is very thick. In thin disk theory, the accretion time scales as  $\alpha^{-1}(z/r)^{-2}$ , where  $\alpha$  is the viscosity parameter,  $z$  is the height of the disk, and  $r$  is the radial distance. The thicker the disk, the faster it accretes.

The outline of the paper is as follows. In § 2, we provide an overview of the novel technique for forming evolutionary sequences out of hydrostatic models of thick accretion disks. The method relies primarily on global conservation laws and the assumption that the viscosity is everywhere positive. In § 3, we describe the hydrostatic models which compose the evolutionary sequence. The method for evolving the models in time is presented in § 4. Initial conditions are given in § 5 for the evolutionary sequences. In § 6, we present results, including discussions of the energy spectrum, the residual mass, and the importance of the inner nozzle. Long-term emission properties of thin disks which form after the thick disk phase are described in § 7. Conclusions are given in § 8.

## 2. Method Overview

Here we investigate what ensues after the formation of a thick disk created from the debris of the tidal disruption of a star by a massive black hole. In such an event, it is believed that a fraction of the stellar debris will be deposited in an accretion disk around the massive black hole.

The evolution of these thick, radiation-pressure-dominated disks is studied as they generically expand, accrete onto the black hole, and transfer angular momentum outwards. Often, the thick disk expands, begins to accrete, and after a fraction of the disk accretes onto the black hole, the disk becomes thin. The evolution is followed until the disks become thin.

The method is to construct hydrostatic models of thick disks using a small number of parameters to specify the structure of the disk. These models are then formed into a time sequence in which the global quantities of mass, angular momentum, and energy are conserved. Viscosity is required to be positive, but not constant as a function of radius or

time. The run of viscosity with radius is set by the time sequence of models, as opposed to conventional methods in which the standard viscosity parameter,  $\alpha$ , is specified and taken as constant throughout the disk. Time varying  $\alpha$  has been commonly invoked in the study of dwarf-novae (e.g. Cannizzo, Shafter, & Wheeler 1988, Livio & Spruit 1991) as has radial variation in  $\alpha$  (Smak 1984, Cannizzo, Wheeler, & Polidan 1986); this paper’s method is well suited to this general case. The range of allowable time sequences is investigated to determine limits on relevant physical parameters such as the efficiency of conversion of gravitational binding energy to radiation and of the amount of disk mass left after the thick disk phase. It is also possible to evaluate the importance of initial values to the problem such as the pericenter of the disrupted star and the mass of the black hole. Our approach is similar to that of Abramowicz, Henderson, and Ghosh (1983) who formed sequences of hydrostatic thick disk models, by first assuming a constant viscosity parameter,  $\alpha$ , and then evolving the disk according to global conservation laws.

The hydrostatic models for non-accreting disks have four free parameters: the inner radius of the disk, a polytropic constant which is related to the ratio of gas pressure to radiation pressure, and two additional parameters which specify the run of angular momentum with radius. For accreting disks, it is necessary to specify only one parameter for the run of angular momentum. The models are described in detail below.

### 3. Hydrostatic Models

For most the models we consider, the timescale for evolution of the disks is much longer than the orbital time, so we construct hydrostatic models (see, for example, Paczyński and Wiita 1980, hereafter PW). Neglecting the time dependence in the disk equations is a good approximation unless the local viscous term,  $\alpha$ , approaches unity. Additionally, there are non-hydrostatic effects of accretion at the inner nozzle which we discuss in § 6.3.

To approximate the effect of the Schwarzschild geometry, we use the gravitational potential described in (PW):

$$\Psi = -\frac{GM}{R - R_S}, \quad R_S = \frac{2GM}{c^2}. \quad (3)$$

The Keplerian angular momentum in this potential is

$$j_{\text{Kep}} = (GMR)^{1/2} \frac{R}{R - R_S}. \quad (4)$$

The Newtonian potential and angular momentum are  $-GM/R$  and  $(GMR)^{1/2}$ . Both the Schwarzschild geometry and the PW potential differ from the Newtonian potential in that

there is a marginally stable orbit,  $R_{\text{ms}} = 3R_{\text{S}}$ , and a marginally bound orbit,  $R_{\text{mb}} = 2R_{\text{S}}$ . The marginally stable orbit occurs because angular momentum increases with decreasing radius when  $R < R_{\text{ms}}$ ; the binding energy, or the sum of the kinetic and potential energies, reaches a minimum at  $R_{\text{ms}}$ . The binding energy reaches zero at  $R_{\text{mb}}$ . Keplerian thin disks can extend inwards only as far as  $R_{\text{ms}}$ , whereas thick disks can reach as far as  $R_{\text{mb}}$  because of pressure gradients. We make no further attempt to account for other general or special relativistic effects, which we believe do not qualitatively affect any of the paper’s results and may only slightly affect the quantitative results. (For example, the accretion efficiency of a thin disk is 5.7% whereas the PW potential yields an efficiency of 6.3%.)

The first free parameter of the hydrostatic models is the inner radius,  $r_{\text{i}}$ , where  $r_{\text{i}} > R_{\text{mb}}$ . The structure of a thick disk is fully determined by the run of angular momentum with radius,  $j(r)$ , at the surface. In order for a disk to be dynamically stable angular momentum must increase with radius, so we require the angular momentum distributions to satisfy this constraint.

For the models studied here, we take a modified power law angular momentum distribution as a function with two parameters,  $r_{\text{c}}$  and  $b$ :

$$\begin{aligned} j(r) &= A(r_{\text{c}}, b)r^{b-0.5}j_{\text{Kep}}(r) & \text{for } r > r_{\text{b}} & \quad (5) \\ j(r) &= j(r_{\text{b}}) & \text{for } r < r_{\text{b}}, & \quad (6) \end{aligned}$$

where the constant  $r_{\text{b}}/r_{\text{S}} = 1/(1 + b)$  ensures that  $\partial j/\partial r \geq 0$  for all  $r$ . Examples of angular momentum distributions are shown in figure 1. The slope,  $b$ , ranges between 0.5, where  $j(r)$  is Keplerian, and 0.0, where the angular momentum distribution is flat. The constant,  $A$ , is chosen so that the angular momentum is equal to Keplerian at a specified central radius,  $r_{\text{c}}$ . For  $r < r_{\text{c}}$ , the angular momentum is greater than Keplerian and pressure gradients apply a force inwards. For  $r > r_{\text{c}}$ , the angular momentum is less than Keplerian and pressure gradients apply a force outwards.

For hydrostatic thick disks which are (slowly) accreting, there is a natural constraint on the angular momentum distribution (Abramowicz, Jarosynski, and Sikora 1978). The angular momentum at the inner radius,  $r_{\text{i}}$ , must be Keplerian and  $r_{\text{i}} \leq 3R_{\text{S}} = R_{\text{mb}}$ . For a non-accreting thick disk, the inner radius can extend inwards of  $R_{\text{mb}}$  only as long as the  $j(r) > j_{\text{Kep}}(r)$ . When  $j(r)$  falls below  $j_{\text{Kep}}(r)$ , orbits become unstable.

The last free parameter is related to the equation of state of the gas. It is convenient to assume a polytropic equation of state. Here we take

$$P = K\rho^{4/3}, \quad (7)$$

where  $K$ , the polytropic constant, is taken to be the same everywhere in the disk at a given

instant of time. This approximation is explained in § 4.3. The barytropic equation of state enforces uniform rotation on cylinders.

Equations for hydrostatic equilibrium can be solved as a function of the four parameters,  $r_i, r_c, b$ , and  $K$ . We adopt a convention of lowercase  $r$  for cylindrical radial distance and an uppercase  $R$  for the spherical radial distance.

In the equatorial plane, the radial force balance equation is

$$\frac{1}{\rho} \frac{\partial P}{\partial r} = \frac{\partial \Psi}{\partial r} + \frac{v^2}{r}, \quad (8)$$

where

$$v = \frac{j}{r}. \quad (9)$$

The vertical force balance is

$$-\sin(\theta) \frac{\partial \Psi}{\partial R} + \frac{1}{\rho} \frac{\partial P}{\partial z} = 0. \quad (10)$$

The enthalpy,  $H(r)$ , can be introduced and evaluated as

$$H(r) = \int \frac{dP}{\rho} = 4K\rho^{1/3} = 4\frac{P}{\rho}, \quad (11)$$

for our equation of state (Eq. 7). With equation 8 this can be written,

$$H(r) = \Psi(r) - \Psi(r_i) + \int_{r_i}^r \frac{j^2}{r^3} dr. \quad (12)$$

The differential equation 10 can be integrated to yield

$$\rho = \left[ \frac{1}{K^3} \right] \left[ \frac{c_1}{4} + \frac{GM}{4(R - R_S)} \right]^3, \quad (13)$$

where  $c_1$  is constant on cylinders given by

$$c_1 = 4K\rho_0^{1/3}(r) - \frac{GM}{r - R_S} = H(r) - \frac{GM}{r - R_S}, \quad (14)$$

and  $\rho_0$  is the density in the equatorial plane.

The disk surface is given by

$$z_{\text{sur}}(r) = \left\{ \left[ \frac{r_i - R_S}{1 - \frac{(r_i - R_S)}{GM} \int_{r_i}^r j^2 / r^3} \right]^2 - r^2 \right\}^{1/2} \quad (15)$$

With the density and run of angular momentum determined, most physical quantities of the disk can be obtained from integrations (either numerical or analytical). The disk mass and angular momentum are

$$M = \int_{r_i}^{r_e} 2\pi r \Sigma dr \quad (16)$$

$$J = \int_{r_i}^{r_e} 2\pi r \Sigma j dr \quad (17)$$

The total disk energy is the sum of potential, kinetic, and internal energies (self-gravity is negligible):

$$E_{\text{kin}} = \int_{r_i}^{r_e} \frac{2\pi r \Sigma j^2}{2r^2} dr \quad (18)$$

$$E_{\text{pot}} = \int_{r_i}^{r_e} 2 \int_0^{z_{\text{max}}} 2\pi r \frac{GM\rho}{R - R_S} dz dr \quad (19)$$

$$E_{\text{in}} = \int_{r_i}^{r_e} 2\pi r \left(3 - \frac{3}{2}\beta\right) 2 \int_0^{z_{\text{max}}} P(r, z) dz dr, \quad (20)$$

where  $\beta$  is the ratio of gas pressure to total pressure and is directly related to the polytropic constant,  $K$ . The disk luminosity can be determined if we assume that the disk atmosphere, which is radiation pressure dominated, is radiating critically like high-mass stars, so they can be described by an Eddington model:

$$F_{\text{rad}} = (1 - \beta) \frac{c}{\kappa} g_{\text{eff}}, \quad (21)$$

where  $\kappa$  is the opacity per gram and  $g_{\text{eff}}$  is the effective acceleration (including centrifugal force). Integrating over the surface of the disk, the luminosity is (PW)

$$L_{\text{rad}} = 2 \int_0^{2\pi} \int_{r_i}^{r_e} d\sigma \quad (22)$$

$$= (1 - \beta) \frac{4\pi GMc}{\kappa} \int_{r_i}^{r_e} \left[ \frac{j^4 R(R-1)^2}{G^2 M^2 z r^5} - \frac{2j^2}{GMzr} + \frac{rR}{z(R-R_S)^2} \right] dr, \quad (23)$$

where  $\sigma$  is the element of surface area. The luminosity may be altered by strong winds (e.g. U97) as well as by effects in the funnel (e.g. Nityananda & Narayan 1982), but for the purposes of this paper we calculate the luminosity with Eq. 22. Figure 2 and figure 3 show many examples of these hydrostatic models.

#### 4. Evolution in Time

Our goal is to form time sequences of hydrostatic models under four physical constraints: global mass conservation, global angular momentum conservation, global

energy conservation, and positive local viscosity. A computer code was written to perform the necessary numerical integrations for mass, angular momentum, energy, etc. Additionally, it imposes the physical constraints and forms time sequences of models. The physical constraints greatly reduce the degrees of freedom in the four dimensional parameter space as described below.

Mass and angular momentum conservation require that for a non-accreting disk  $M$  and  $J$  are constant between models in a time sequence. For an accreting disk,  $M$  and  $J$  must vary as

$$\Delta J = j(r_i)\Delta M. \quad (24)$$

As discussed above  $j(r_i) = j_{\text{Kep}}(r_i)$ , for accreting disks. The mass of the black hole,  $M_{\text{BH}} \gg M$ , so we take  $M_{\text{BH}} = \text{const}$ . The code ensures that the constraints are met to approximately one part in  $10^6$  per step which far exceeds the necessary accuracy as most evolutionary sequences contain about 100 time steps. The constraints of conserved mass and angular momentum are not necessarily met if winds carry much the disk mass away (e.g. U97). If this is the case, it will be very difficult to detect tidal disruption events from their long-term emission, but the bright flares may be even more optically accessible as the winds may reprocess some of the higher energy photons to optical.

Energy is not conserved in the black hole/disk system because of radiation. However, we use energy conservation to determine the amount of energy radiated between two models and thereby find the time step. For a non-accreting disk,

$$\Delta t = \frac{-\Delta E}{L}, \quad (25)$$

where  $\Delta E$  is determined from equations 18 and we impose the physical requirement that  $\Delta E \leq 0$ . For an accreting disk, the energy of the system changes not only due to radiation but also due to mass loss on to the black hole. In contrast to advection dominated models (e.g Narayan & Yi 1995, Chen et al. 1995) the pressure at the inner radius falls to zero, so accreting matter has negligible internal energy. Therefore, the energy change between steps is

$$\Delta E = -E_{\text{rad}} + \Delta M \left[ \frac{-GM}{r_i - R_S} + \frac{j(r_i)^2}{2r^2} \right]. \quad (26)$$

The constraint of positive viscosity ensures that angular momentum is transferred outwards. Specifically, for angular momentum distributions for which  $\partial\Omega/\partial r \leq 0$  which are of general interest in astrophysics, the torque between two adjacent cylinders is always such that angular momentum is flowing outwards on mass shells. This constraint means that the torque between adjacent cylinders,  $g$ , is greater than zero, so  $\dot{J} - \dot{M}j > 0$ , since  $\dot{J} = \dot{M}j + g$ . Thus, in contrast to the first three constraints, the viscosity constraint needs



to be applied locally. In practice, the constraint is applied at twenty points in the disk which are evenly spaced in mass and include the endpoints.

In geometric terms, the goal is to understand the physically allowable paths that can be taken from an initial starting point in the 4-dimensional parameter space of  $r_i$ , the inner radius;  $r_c$ , the radius at which the angular momentum is equal to the Keplerian value;  $b$ , the slope of the angular momentum distribution; and  $K$ , the polytropic constant. These paths are discussed subsequently.

#### 4.1. Non-Accreting Evolution

The physical constraints greatly limit the possible evolutionary sequences. The two constraints of mass and angular momentum conservation in the non-accreting case reduce the parameter space from four dimensions to a 2-d surface (in 4-d) of models with constant mass and angular momentum. The remaining two constraints from energy conservation and positive viscosity further limit the possible evolutionary sequences, but in a more complex manner.

For purposes of discussion, let us suppose that the energy loss from radiation is negligible so that the disk evolves with constant energy. Then, the allowable parameter space contracts from a surface to a curve. Finally, the requirement that viscosity is positive gives a direction of evolution along the curve, so there is only one physically allowable sequence of models which all lie along the curve.

Figure 4 shows evolution from a narrow torus of matter to a flattened disk in this limit with no radiation loss. Initially, when the angular momentum distribution is flat, the disk's surface has a circular cross section for an infinitely narrow torus as can be analytically demonstrated. As the disk evolves, the circular cross section evolves into an ellipse as the angular momentum distribution steepens. The relationship between the slope of the angular momentum distribution,  $b$ , and the ellipticity is derived analytically in Appendix B. The numerical code well reproduces the relationship predicted by the analytical approximation. Like thin-disks, the non-accreting thick disk spreads inwards and outwards in radius as time progresses.

In the more general and physically applicable case where energy is radiated, the evolutionary sequences are not unique; however, they all lie on the same 2-D surface. The problem can be simplified because the disk is in general spreading both inwards and outwards in radius until it begins to accrete, so the code may take steps at times when  $r_i$  is equal to specified values less than the starting radius. Once  $r_i$  is specified, there is only

one degree of freedom left. The range of possible models can be bracketed in a number of ways. For instance, at each step one can take the minimum and maximum values of the angular momentum slope,  $b_{\min}$  and  $b_{\max}$ , which provide solutions that meet the positive viscosity and energy constraints. Alternatively, the two limiting cases could be taken to be models, denoted  $\Delta E_{\min}$  and  $\Delta E_{\max}$  in which as little or as much energy is radiated as possible between timesteps. Examples of these two limiting cases are shown in figure 5 and figure 6. The two types of bracketing cases are identical for much of the evolution of thick disks, which is to say the limiting cases for  $b_{\min}$  are the same as for  $\Delta E_{\min}$ . The case with  $\Delta E_{\min}$  is one in which as little energy is radiated as possible; and energy is eventually lost through low-efficiency accretion. This limit is of physical interest, because it is the case which determines the minimum accretion efficiency of the tidal disruption events as well as determines the minimum amount of mass which remains in the disk after the thick disk phase. The  $\Delta E_{\max}$  limit is one in which the disk radiates as much energy as possible. For the models we are investigating, the slope,  $b$ , increases far enough that the disk eventually takes a Keplerian angular momentum distribution and becomes essentially thin. While thin disks are not well modeled by the approximations of the code (particularly, the polytropic constant,  $K$ , is not be the same everywhere in the disk), the late stages of evolution of a thin disk around a black hole have been studied by Cannizzo, Lee, & Goodman (1990; hereafter CLG), and we can draw on their work to determine the subsequent evolution.

## 4.2. Accreting Evolution

While the disk is accreting, there are only three free parameters as discussed above, because the angular momentum must be Keplerian at the inner radius,  $r_i$ . This constraint creates an algebraic relationship between  $r_i$ ,  $b$ , and  $r_c$ . Eliminating  $r_c$ , for instance, reduces the parameter space to three dimensions.

Because the disk is accreting, timesteps are taken at specified values of  $M$  less than  $M_{\text{initial}}$  in a similar fashion to how timesteps were taken at given values of  $r_i$  in the non-accreting case. The mass and angular momentum constraints,  $\Delta M_n = M_{n-1} - M_n$  and  $\Delta J_n = j(r_i)\Delta M_n$ , can then be used to reduce the three dimensional space to a one-dimensional space. As for the non-accreting case, we are left with the task of bracketing the possible evolutionary tracks that are allowed within the constraints of energy loss and positive viscosity.

One possible way to bracket the range of time sequences is to take extreme values of  $r_i$  at each step. This limit is computationally convenient because  $r_i$  is always between 2 and 3  $R_S$  in the accreting case. It is a physically interesting limit because the efficiency and

disk structure are strongly tied to the inner radius. In particular, the total efficiency of the accretion process determined by the effective potential at  $r_i$  and is given by

$$\epsilon = \frac{1}{m_0 c^2} \int_{t_i}^{t_f} L(t) dt \approx -\frac{1}{m_0 c^2} \left\{ \int_{t_i}^{t_f} \left[ -\frac{GM_{\text{BH}}}{r_i(t) - R_S} + \frac{j(t)^2}{2r_i(t)^2} \right] \frac{dM_d}{dt} dt \right\}, \quad (27)$$

where an initial disk of mass,  $m_0$ , accretes at a rate of  $\partial m / \partial t(t)$  and radiates at a luminosity,  $L(t)$  from time  $t_i$  to time  $t_f$ . As discussed in PW with reference to steady-state models, because the effective potential (enclosed in brackets in Eq. 27) rises from a minimum at  $3R_S$  to zero at the marginally bound orbit,  $2R_S$ , the more mass lost at small  $r_i$ , the lower the efficiency. The full general relativistic treatment for a non-rotating black hole has the same qualitative features and is quantitatively well approximated by the potential of PW (e.g.  $\epsilon_{\text{max,S}} / \epsilon_{\text{max,PW}} \sim 1.1$ ).

### 4.3. Additional Constraints

Additional constraints can be placed on the disk evolution to make the evolution more physically realistic. We discuss two constraints, one of which is related to the local viscosity, and the second to the thermal timescale.

We may wish to place limits on the local or average value of the viscosity. For instance when the strength of the viscosity is parameterized with  $\alpha$ , i.e.  $\eta = \alpha \eta_{\text{max}} = \frac{2}{3} \alpha \rho v_s z_0$ ,  $\alpha$  should always be less than 1. Additionally, when  $\alpha$  approaches unity, neglect of the time-dependent terms in the momentum-balance equations may become a poor approximation.

Positive viscosity is enforced from timestep to timestep. The viscosity varies with radius and time in contrast to most approximations (e.g. standard  $\alpha$ -disk theory). The local viscosity can be determined from the relation,  $\dot{J} = \dot{M} j + g$ , since  $\dot{J}$  and  $\dot{M}$  (averaged over the timestep) can be determined at each radius. The torque can be approximated by  $g \approx -\alpha 2\pi r^3 \Sigma v_s 2z_{\text{sur}} \partial \Omega / \partial r$ . In this manner,  $\alpha$ , can be determined as a function of time and radius. At each timestep, additional constraints can be placed on  $\alpha$ . For instance,  $\alpha$  is required to be less than 1, and in some cases, the mass weighted value of  $\alpha$  is required to lie within a certain range.

A second constraint can be applied to enforce the the assumption that the disk is a constant entropy polytrope. The assumption requires that heat be exchanged rapidly within the disk, because at large radii, the energy radiated is larger than the energy locally dissipated (and vice-versa for small radii). The energy radiated in a shell (Eqs. 21-22) goes

as  $rg_{\text{eff}} \approx r^{-1}$ . The energy dissipated per unit volume is approximately

$$E_{\text{dis}} \approx \left( r \frac{d\Omega}{dr} \right)^2 \alpha \Sigma v_s \approx r^{2b-4} \alpha \Sigma v_s, \quad (28)$$

which is generally a sharply falling function of radius, since  $b$  is between 0 and 0.5, and  $\Sigma$ ,  $v_s$ , and even  $\alpha$ , generally decrease with radius for  $r > r_c$ . Energy could be transported with the disk either through circulation patterns which are limited by the sound speed, and which can be very efficient as shown by contact binaries (see explanation by Tassoul 1992, and references therein) or by radiative diffusion which is limited by the diffusion speed,  $\sim c/\tau$ , where  $\tau$  is the optical depth between the points of energy transfer. Radiative diffusion may become the dominate heat transfer mechanism at very large radii as the density falls. Rather than model the radiative diffusion or a circulation pattern, we consider two cases with the numerical code: (1) the two mechanisms together are efficient enough to keep the disk in a constant entropy state or (2) the heat transfer is limited at a critical radius where the time for heat to be transferred by circulation patterns exceeds the Kelvin-Helmholtz time. The transfer time is estimated as

$$t_{\text{trans}}(r) \approx \int_{r_c}^r \frac{dr}{v_s}. \quad (29)$$

In the second case, we keep track of the amount of matter outside of the critical radius and assume that it collapses to a thin disk on the Kelvin-Helmholtz timescale. Once in a thin disk, the matter is ignored for the remainder of the evolution. In practice, there is very little difference between the main results (§ 6) in of both cases.

## 5. Initial Conditions

We run the simulations for three black hole masses,  $10^6$ ,  $10^{6.5}$ , and  $10^7 M_\odot$  to cover the range of black hole masses about which thick disks are likely to form. Because angular momentum is lost when the star disrupts, the mean angular momentum of the initial disk is the same as that of the star. If the debris circularizes into a narrow torus, then the torus would have radius,  $2R_p$ , where  $R_p$  is the pericenter of the star’s orbit. We consider disks with mean angular momentum corresponding to disruptions at 0.5, 1, and 2  $R_t$ , where  $R_t$  is the the tidal radius. The debris is taken initially to have constant specific angular momentum, as might be expected since the debris does have constant angular momentum when the star is disrupted and if shocks efficiently circularize the debris, then energy may be more readily transferred than angular momentum. We begin the evolution with a high internal energy state, where  $r_i \approx r_c/2$ , but the results are not very sensitive to this condition

( $\sim 10\%$  difference in the physical parameters discussed below). Nevertheless, there is some uncertainty in the initial angular momentum state of the disk.

The simulations are most applicable to disruptions around black holes with masses below  $\sim 10^7 M_\odot$ . The simulations begin with a debris torus which subsequently accretes at Eddington and super-Eddington accretion rates; however, the marginally bound disruption debris only gradually returns and circularizes on a timescale  $t_{\min}$  (eq. 2). For black holes above  $\sim 2 \times 10^7 M_\odot$ , the circularization timescale becomes so long that material enters the disk at a rate slower than required to fuel the black hole at the Eddington rate (U97). For these systems, thick disks cannot form.

For the lower mass black holes, even if the material is returned at a high enough rate to fuel the black hole above the Eddington limit, the accretion rate may be so high that much of the material accretes before all of the debris is circularized (U97). In this case, which appears to generally occur when  $\alpha \gtrsim 0.01$ , much of the debris settles into the disk while the disk is accreting. This returning matter cannot be directly accounted for with the current simulations.

We address the problem with two types of runs. First, as described in § 4.3, we can impose a restriction on the mass weighted viscosity parameter so that the accretion times are not so fast as to drain the disk before the material circularizes. These are the runs labeled “a” in Tables 1-3. Second, we can evolve a thick disk with as high viscosity as physically possible, even though in reality the disk could not have fully circularized. Such sequences may approximate the evolution when material is gradually fed to the disk, because such simulations have the same mean angular momentum, and it appears that the angular momentum is the most important parameter in the problem. In these runs, the viscosity generally varies from near unity at the innermost radius to a 0.1 at large radii. These runs are marked “c.”

## 6. Results

The results from a variety of evolutionary tracks are shown in Tables 1-3. The evolution is followed from the initial conditions given in § 5 to a state in which the disk is no longer thick. An appropriate cutoff is when the slope,  $b$  becomes larger than 0.48, where 0.5 corresponds to a Keplerian thin disk. The evolutionary sequences are calculated with a variety of combinations of the additional constraints of § 4.3 to investigate their effects on the main results.

As explained in § 4.1, in one type of physically allowed evolutionary track, the disk

cools quickly and forms a thin disk. Thin disk evolution has been studied by CLG. If the disk cools quickly ( $\alpha$  is small), there would likely be a relatively bright period of 1-3 years when the disk shines below the Eddington luminosity, followed by a self-similar phase in which the luminosity falls off as  $\sim t^{-1.2}$ . The long-term evolution of disks is discussed in § 7.

The main type of evolutionary track we study is one in which the disk accretes quickly. In these tracks, the maximum amount of mass is accreted onto the black hole before the disks become thin. The disks can accrete extremely fast, so if the viscosity is large enough in the disks for such quick evolution, the accretion may be limited by circularization of material which takes at least  $t_{\min}$  (eq. 2). Similarly, the efficiency of the accretion can become extremely small in the idealized case where the all of the debris begins in a circularized disk and it accretes at the maximum rate (“b” and “c” in tables 1-3). The pericenter of the stellar orbit is important in determining how much of the disk can be accreted as can be seen by the strong correlation between residual mass and pericenter, as is explained in § 6.2. For the same reason, there is an inverse relationship between the black hole mass and the residual mass.

## 6.1. Spectra

The spectra of the disks may be calculated at each time step under the assumption that the surface is a thermal. The optical depth is quite large,  $\sim 10^6$ , even to Thompson scattering, so the radiation from the disk surface is most likely thermal. With the the local luminosity specified by eqs 22, the local temperature may be determined with the Stefan-Boltzmann law. A Planck function is used to describe the local emission, and is integrated over the disk surface to determine the final spectrum. If as we believe, the scattering cross-section far exceeds the absorption cross-section, the local spectrum could be better described with a Wien peak and a modified black body spectrum (e.g. Rybicki & Lightman 1979). Given the ad hoc nature of the angular momentum distribution and uncertainties in the structure of the inner funnel of the disk (e.g. Nityananda & Narayan 1982), such refinements are unwarranted.

Results of such calculations are presented in U97, along with a description of current uncertainties which may affect the energy spectrum. As discussed in U97, the viewing angle of the disk is very important because much of the emission is radiated from the inner regions of the disk which are not visible to an edge-on viewer. The edge-on disk is  $\sim 50$  times less luminous than the face-on disk, although because the outer disk is much cooler than the inner disk, the difference seen in the optical bands may be significantly less,  $\sim 5$ . Viewed face-on, the bolometric luminosities are a few times the Eddington limit, but the

spectra are very hot, peaking between 50 and 100 eV. The estimated bolometric corrections for U and V are  $\sim 5.5$  and  $7.5$ , respectively.

## 6.2. Residual Mass

In most cases a significant fraction of the mass of the thick disk cools and forms a thin disk around the black hole, where it accretes on a longer timescale (tables 1-3). The main reason why mass cannot be fully accreted in the thick disk is that the specific angular momentum of the disk rises as the disk accretes, so the disk must spread to large radii. The specific angular momentum of material which accretes onto the black hole is generally much smaller than the mean angular momentum of material in the disk. For example, the disk formed by a solar-type star with pericenter equal to the tidal radius which is disrupted by a  $10^6 M_\odot$  black hole has mean specific angular momentum  $10GM_{\text{BH}}/c$ , whereas the angular momentum of the accreting material, has specific angular momentum

$$\frac{\sqrt{2}(r_i/R_S)^{3/2}}{(r_i/R_S) - 1} \frac{GM_{\text{BH}}}{c} < 4 \frac{GM_{\text{BH}}}{c}. \quad (30)$$

If 50% of the disk accretes, then the average specific angular momentum of the remaining material must increase to  $\sim 16$ , increasing the mean distance of the disk as well as the accretion timescales for the remaining material. More generally, if a fraction,  $x$ , of the disk accretes with a specific angular momentum,  $4GM_{\text{BH}}/c$ , then

$$j_f = \frac{j_i - x4GM_{\text{BH}}/c}{1 - x}. \quad (31)$$

As the specific angular momentum of the disk grows, so does its characteristic radius,  $r \propto j_f^2$  and the accretion timescale,  $t \propto r^{3/2} \propto j_f^3$ . Therefore, when 90% of the mass is accreted, the mass accretion rate has fallen by  $\sim 1000$ . Thick disks only exist in steady-state when the accretion rate is super-Eddington, so the disks will generally cool to form thin disks before accreting a large fraction, e.g.  $> 90\%$ , of the disk. The exceptions in Table 3 occur when the initial angular momentum (and therefore pericenter) of the star is small. In fact, when the initial mean angular momentum of the disk approaches that of the Keplerian angular momentum at marginally bound orbit, the disk can gain very little specific angular momentum as it accretes. The initial mean angular momentum will be this low when the encounters are very close with  $R_p \approx 2.5$ , which may not be uncommon among disruption events around black holes with  $M \gtrsim 10^7 M_\odot$ .

### 6.3. Inner Nozzle

While hydrostatic solutions have no inner nozzle, physically realistic accreting solutions must have an opening at the inner radius. Because of the importance of the inner radius in determining the efficiency of the accretion, an understanding of the inner nozzle is vital. In general, the structure of the inner nozzle depends on the angular momentum at the inner radius, the mass accretion rate, and the polytropic constant,  $K$ .

The problem of an inner nozzle for thick disks has been addressed in a number of ways. For instance, Loska (1981), solves vertically integrated equations under the assumptions of vertical hydrostatic equilibrium, that  $z/r_i \ll 1$ , and that the radial velocity of matter is dependent only on the  $r$ -coordinate. The critical point for the flow is extremely close ( $< 10^{-4}r_i$ ), to the inner radius without the nozzle, for the solutions described by Loska. The solutions have no simple scaling relation; however, utilizing the fact that the critical point is extremely close to the inner radius justifies a slight simplification of the problem which provides scaling laws.

In appendix B, we apply an approach similar to that of Paczyński and Sienkiewicz (1972) who addressed the Roche lobe nozzle in contact binaries. All of the physical quantities calculated in the code may be determined for a disk with a nozzle, with knowledge of the height of the nozzle (half-thickness of the disk) which obeys the scaling relation (Appendix B):

$$z_s \propto \dot{M}^{1/8} K^{3/8} r_i^{5/16} (r_i - 1)^{7/8} M_{\text{BH}}^{-1/4}, \quad (32)$$

so the dependences on physical parameters, especially mass accretion rates, are weak.

The disks with nozzles differ only slightly from those without. Even for the fastest accreting models, the residual mass (§ 6.2) differs only by  $\sim 10 - 20\%$ . The main difference in the models with inner nozzles is that the efficiency of accretion is reduced, in some cases by a factor of two because kinetic energy is advected into the black hole.

## 7. Long-term Evolution

After the disk becomes thin, the evolution can no longer be tracked by the thick disk evolutionary code. To determine the long-term evolution, we begin with the scaling relations derived by CLG for thin disks which, in part, draw upon the self-similar solutions of Pringle (1974). The mass accretion rate onto the black hole according to their scaling



relations (their eqns 17 and 18) and normalized to their numerical results is

$$\dot{m} \approx 1.5 \times 10^{25} A^{7/8} \left(\frac{\alpha}{0.1}\right)^{-1/4} \left(\frac{M_d(0)}{0.5M_\odot}\right)^{7/8} \left(\frac{M_{\text{BH}}}{10^7 M_\odot}\right)^{5/24} \left(\frac{t}{\text{1year}}\right)^{-19/16} \text{ gm s}^{-1}, \quad (33)$$

where  $M_d(0)$  is the initial mass of the disk, and  $A$  is the ratio of mean angular momentum of the disk to mean angular momentum of a star with pericenter equal to the tidal radius, and is  $\sim 0.5 - 1.5$  initially. If no angular momentum were carried into the black hole,  $AM_d(0)$  would be constant as the disk accretes. The results of § 6 may be applied to the long term evolution by using the final state of the thick accretion disk as the starting point for the thin disk similarity solutions. The necessary parameters are the mass and mean angular momentum of the residual disk. Using Eq. 33, both the luminosity as a function of time and possible transitions to an less-efficient advection dominated regime may be evaluated. The evolution of the thin disk luminosity was determined by CLG. They characterized the duration of the long-term *bolometric* luminosity with the time,  $t_1$ , at which  $L_{\text{bol}}/M_{\text{BH}} = L_\odot/M_\odot$  and found it could be many thousand years. Initially, the thin (and thick disks) are extremely hot and radiate only a small fraction,  $\lesssim 1\%$ , of their luminosity in the optical (see CLG and U97). After 3000 years, CLG find that the peak of the broad flux distribution shifts to 2000 Å, so a much larger fraction of light is emitted in the optical. Assuming an efficiency of 6% for conversion of mass to energy, as is appropriate for thin disks around Schwarzschild black holes, the disk will remain optically bright for (CLG)

$$t_1 \approx 5000 f(t)^{16/19} A^{14/19} \left(\frac{\alpha}{0.1}\right)^{-4/19} \left(\frac{M_d(0)}{0.5M_\odot}\right)^{14/19} \left(\frac{M_{\text{BH}}}{10^7 M_\odot}\right)^{-2/3} \text{ years}, \quad (34)$$

where  $f(t)$  which accounts for the relative brightness of stars and the disk in the spectral band of choice; it is the ratio of the fraction of disk light emitted in the band to the fraction of stellar light emitted in the band, and is close to 1 in the optical after 3000 years.

We may now ask the question of how an early thick disk phase could affect the long-term emission by applying Eq. 34 to the thin disks which remain after the thick disk phase. The results are shown in Tables 1-3. The timescales for dimming are extremely long. If the tidal disruption rate in a typical galactic nuclei is  $\sim 10^{-4} \text{ yr}^{-1}$  and the thin disks accrete with efficiency 6%, then lower mass black holes would be in a near constant state of emission.

If the accretion rate drops low enough, the accretion disk may become advectively dominated. Advection would reduce the efficiency of the accretion process below 6% and could move much of the emission to a higher temperature out of the optical band. The disk may become advective when the mass accretion rate drops below a critical value,

$\dot{M}_{\text{crit}} \approx 10 \alpha^2 L_{\text{Edd}}/c^2$ . For a number of advective systems,  $\dot{M}_{\text{crit}} \approx 0.1 L_{\text{Edd}}/c^2$  (e.g. Narayan 1996) The time at which the accretion may become advective according to Eq 33 is

$$t_{\text{adv}} \approx 40 A^{14/19} \left(\frac{\alpha}{0.1}\right)^{-36/19} \left(\frac{M_{\text{d}}(0)}{0.5M_{\odot}}\right)^{14/19} \left(\frac{M_{\text{BH}}}{10^7 M_{\odot}}\right)^{-2/3} \text{ years.} \quad (35)$$

Below the critical mass accretion rate, the luminosity falls as  $\sim \dot{M}^2$ . If the mass accretion rate continues to follow the same form as Eq. 33, then the point at which the bolometric luminosity falls below  $M_{\text{BH}}L_{\odot}/M_{\odot}$  is

$$t_2 \approx 400 A^{14/19} \left(\frac{\alpha}{0.1}\right)^{-20/19} \left(\frac{M_{\text{d}}(0)}{0.5M_{\odot}}\right)^{14/19} \left(\frac{M_{\text{BH}}}{10^7 M_{\odot}}\right)^{-2/3} \text{ years.} \quad (36)$$

Tables 1-3 shown that even in the advection dominated case, the black holes will stay bright for an extended period of time. For  $10^7 M_{\odot}$  black holes, the disk will dim on the timescale of  $\sim 200(0.1/\alpha)$  years, whereas for  $10^6 M_{\odot}$  black holes, the disk may remain bright 10 times as long even when advection dominated.

The self-similar solution does not account for the loosely bound debris of the initial disruption which slowly rains down on the disk as  $\dot{M} \sim t^{5/3}$  (Rees 1988, Phinney 1989), but the return rate of the marginally bound material falls below that of the accretion rate from the self-similar solution within the first year. We conclude that the long-term emission will be determined by the evolution of the thin disk and not by return of marginally bound material in agreement with CLG.

## 8. Conclusions

Only a fraction of the disk mass can be consumed in the initial thick disk phase, which is likely to occur for tidal disruptions around  $10^6 - 10^7 M_{\odot}$  black holes. This fraction ranges from  $\sim 0 - 0.99$  for disruptions around  $10^6$  to  $10^7 M_{\odot}$  black holes, and has a typical value of  $0.5 - 0.9$ . The amount of the residual mass decreases for larger mass black holes and increases with the pericenter of the disrupted star. This residual material will accrete in a thin disk over a longer period of time. The existence of the initial thick disk phase may reduce the dimming timescale of the disk by a factor of  $\sim 2$  from estimates based on thin disks alone. Assuming that an  $0.5M_{\odot}$  initial thick disk, even if the thin disks become advection dominated, the black hole mass to light ratio can rise above  $M_{\odot}/L_{\odot} = 1$  in no less than  $20 (0.1/\alpha)$  to  $2000 (0.1/\alpha)$  years following a tidal disruption event, depending on the black hole mass and initial orbital of the disrupted star. The long-term emission will be most prevalent around  $10^6 M_{\odot}$  black holes. If the tidal disruption rates in these galactic

nuclei are  $\sim 10^{-4} \text{ yr}^{-1}$ , then at least  $\sim 10\%$  of the nuclei should exhibit the long-term UV/optical emission at a level of  $\sim 10^{38} \text{ ergs s}^{-1}$ .

I thank Jeremy Goodman, Bohdan Paczyński, and David Spergel for many helpful suggestions on this work. AU was supported by an NSF graduate fellowship and NSF grants AST93-13620 and AST95-30478.

## 9. Appendix A

In this appendix, the evolution of an infinitely narrow torus with constant angular momentum is investigated. This example can be evaluated in large part analytically and therefore offers a check on the the numerical analysis used elsewhere in the paper.

A thick disk with constant angular momentum and barytropic equation of state of infinitesimal width in a Newtonian potential has equipotentials (including the surface) that are circular in cross-section. For example, at the surface of such a circular-cross-section disk,

$$z^2 + (r - (r_i + \Delta))^2 = \Delta^2, \quad (37)$$

where the disk is centered on  $(r_i + \Delta)$  and the torus has radius  $\Delta = (r_e - r_i)/2$ .

More generally, we show that when the angular momentum is not constant with radius, but rather a power law, the equipotentials are ellipses. At the surface of the disk (see section 3)

$$z = \left\{ \left[ \frac{r_i - R_S}{1 - \frac{(r_i - R_S)}{GM} \int_{r_i}^r j^2 / r^3 dr} \right]^2 - r^2 \right\}^{1/2}. \quad (38)$$

For simplicity, the calculations are performed in a Newtonian potential, ( $R_S/r_i \ll 1$ ), the angular momentum is a power law with radius, ( $j = Ar^b$ ), and the distance between the inner and outer radii is  $2\Delta$ .

Within this framework, the equation for the surface is

$$z = \left\{ \left[ \frac{r_i}{1 - \frac{r_i}{GM} \int_{r_i}^r A^2 r^{2b-3} dr} \right]^2 - r^2 \right\}^{1/2} \quad (39)$$

$$z^2 = \left[ \frac{r_i}{1 - \frac{r_i^{2b-2} A^2}{GM(2b-3)} \left( \left( \frac{r}{r_i} \right)^{2b-3} - 1 \right)} \right]^2 - r^2 \quad (40)$$

The amplitude of the angular momentum,  $A$ , is such that the angular momentum is Keplerian at the center of the disk,  $r_i + \Delta$ :

$$A = (r_i + \Delta)^{1/2-b}. \quad (41)$$

The powers of  $A$  that are needed for the calculation, expanded to first order in  $\delta = \Delta/r_i$  are

$$A = r_i^{1/2-b}(1 + (1/2 - b)\delta) \quad (42)$$

$$A^2 = r_i^{1-2b}(1 + (1 - 2b)\delta) \quad (43)$$

$$A^4 = r_i^{2-4b}(1 + (2 - 4b)\delta). \quad (44)$$

Writing  $r$  as  $r_i + \epsilon$ , where  $-\Delta < \epsilon < \Delta$ , substituting into Eq. 40, and expanding to second order in  $\epsilon/r_i$  and  $\Delta/r_i$  yields

$$z^2 = r_i^2 \left( 1 + 2\frac{\epsilon}{r_i} + 2(1 - 2b)\frac{\Delta\epsilon}{r_i^2} + 2b\frac{\epsilon^2}{r_i^2} \right) - r^2 \quad (45)$$

Replacing  $\epsilon$  with  $r - r_i$  and expanding terms

$$z^2 = (-1 + 2b)(r_i^2 + r^2 + 2r\Delta - 2rr_i - 2r_i\Delta) \quad (46)$$

$$z^2 + (-1 + 2b)\Delta^2 = (-1 + 2b)(r - r_i - \Delta)^2 \quad (47)$$

$$\frac{z^2}{1 - 2b} + (r - r_i - \Delta)^2 = \Delta^2. \quad (48)$$

The shape of the surface (and equipotentials) ranges from a circle when  $b = 0$  to a thin disk or line when  $b = 0.5$ , corresponding to Keplerian rotation.

As expected, the code utilized in earlier sections produces ellipsoidal cross sections with the correct ellipticity. As a non-accreting disk evolves, the inner-edge moves inwards and the outer edge moves outwards. As the disk expands, it flattens. Equation 48 is a good description of disk equipotentials when both  $R_S/r_i$  and  $(r_e - r_i)/r_i$  are small.

## 10. Appendix B

In this appendix, we derive a useful scaling relationship for the thickness of the nozzle. We operate under the assumptions of Loska (1981), who solved vertically integrated equations under the following assumptions: the disk is in vertical hydrostatic equilibrium,  $z/r_i \ll 1$ , and the disk is polytropic. According to Loska, the critical point for the flow is extremely close ( $< 10^{-4}r_i$ ), to the inner radius without the nozzle, but the solutions have no simple scaling relation. The proximity of the critical point to the inner radius justifies

a slight simplification of the problem which provides scaling laws. We follow an approach similar to that of Paczyński and Sienkiewicz (1972) who addressed the Roche lobe nozzle in contact binaries.

In absence of accretion, the disk forms a cusp at  $r_i$ . We expand the effective potential around this point, fixing  $r = r_i$ :

$$\phi = \phi_0[1 + az^2] + \frac{j^2}{2r_i}, \quad (49)$$

where the gravitational potential (PW) is  $\phi_0 = -GM/(r_i - R_S)$ . At the disk surface, the effective potential is

$$\phi_s = \phi_0[1 + az_s^2] + \frac{j^2}{2r_i^2}, \quad (50)$$

where  $z_s$  is the half-thickness of the nozzle, and

$$a = \frac{1}{r_i(r_i - R_S)}. \quad (51)$$

In hydrostatic equilibrium,

$$\frac{dP}{\rho} = -d\phi. \quad (52)$$

Integrating eq. 52 at  $r = r_i$ , with a polytropic equation of state,  $P = K\rho^{1+1/n}$ , yields

$$(n + 1)K\rho^{1/n} + \phi = \phi_{s,\text{hyd}}, \quad (53)$$

where  $(n + 1)K\rho^{1/n} = H(r)$  is the enthalpy (eq. 11), and  $\phi_{s,\text{hyd}}$  is the effective potential evaluated at the the hydrostatic disk's surface. When the material has a constant radial velocity, but maintains its barytropic equation of state, eq. 53 becomes a Bernoulli equation:

$$\frac{1}{2}v^2 + (n + 1)K\rho^{1/n} + \phi = \text{const} \quad (54)$$

If the location of the surface were known, the enthalpy in the equatorial plane can be determined at  $r_i$  (since the value of  $\rho$  in the equatorial plane is known from vertical force balance (eqs. 10,13,14)). Once determined at  $r_i$ , the enthalpy can be found throughout the plane (eq. 12) from which all other physical quantities can be derived. The value of the enthalpy at  $r_i$  is

$$H(r_i) = \frac{GM_{\text{BH}}}{r_i - R_S} - \frac{1}{(r_i^2 + z_s^2)^{1/2} - R_S}. \quad (55)$$

The thickness of the nozzle may be estimated as follows. The flux of matter through the nozzle is limited by

$$F = 4\pi r_i \int_0^{z_s} \rho v_x dz \lesssim 4\pi r_i \int_0^{z_s} \rho v dz. \quad (56)$$

The maximum value of  $\rho v$  may be determined by differentiating eq. 54:

$$v dv + K \frac{n+1}{n} \rho^{1/n-1} d\rho = 0, \quad (57)$$

and using the constraint that at maximum

$$d(\rho v) = 0 = \rho dv + v d\rho. \quad (58)$$

Combining the last two equations with the Bernoulli equation yields

$$(\rho v)_{\max} = \left( \frac{\phi_s - \phi}{n + 0.5} \right)^{n+0.5} \left( \frac{n}{K(n+1)} \right)^n. \quad (59)$$

The flux is then limited to

$$F_{\max} = 4\pi r_i \int_0^{z_s} \left( \frac{\phi_s - \phi}{n + 0.5} \right)^{n+0.5} \left( \frac{n}{K(n+1)} \right)^n dz \quad (60)$$

$$= 4\pi r_i \left( \frac{-\phi_0 a}{n + 0.5} \right)^{n+0.5} \left( \frac{n}{K(n+1)} \right)^n \int_0^{z_s} (z_s^2 - z^2)^{n+1/2} dz \quad (61)$$

$$= 4\pi r_i \left( \frac{-\phi_0 a}{n + 0.5} \right)^{n+0.5} \left( \frac{n}{K(n+1)} \right)^n z_s^{2n+2} C_1, \quad (62)$$

where

$$C_1 = \frac{\sqrt{\pi} \Gamma(1.5 + n)}{2\Gamma(2 + n)} = .429515 \text{ for } n = 3 \quad (63)$$

The true matter flux,  $\dot{m}$  is slightly less than  $F_{\max}$ , but in the case of Roche overflow in binaries, the difference is no more than 20%, a negligible amount considering the crudeness of the assumptions. Nevertheless, a direct calibration on  $\dot{m}/F_{\max}$  with numerical simulations would be welcomed. Simply equating  $\dot{m}$  and  $F_{\max}$  gives an estimate of the nozzle half-thickness

$$z_s = \left[ \frac{\dot{M} K^n}{r_i (-\phi_0 a)^{n+1/2}} \right]^{1/(2n+2)} \left[ \frac{1}{4\pi} \frac{n+1}{n} (n+1/2)^{n+1/2} \frac{1}{C_1} \right]^{1/(2n+2)} \quad (64)$$

For  $n = 3$ ,

$$z_s = 1.56084 \left[ \frac{\dot{M} K^3}{r_i (-\phi_0 a)^{7/2}} \right]^{1/8} \quad (65)$$

$$\propto \dot{M}^{1/8} K^{3/8} r_i^{5/16} (r_i - 1)^{7/8} M_{\text{BH}}^{-1/4} \quad (66)$$

## REFERENCES

- Abramowicz, M. A., Henderson, P. F., & Ghosh, P. 1983 MNRAS 203, 323
- Abramowicz, M. A., Jarosynski, M. & Sikora M., 1978 A&A, 63, 221
- Cannizzo, J. K., Lee, H. M., & Goodman, J. (CLG) 1990, ApJ, 35, 38
- Cannizzo, J. K., Shafter, A. W., & Wheeler, J. C. 1988 ApJ 333, 227
- Cannizzo, J. K., Wheeler, J. C., & Polidan R.S. 1986, ApJ 301, 634
- Chen, X., Abramowicz, M. A., Lasota, J. P., Narayan, R., Yi, I. 1995, ApJ, 443, L61
- Goodman, J.G. & Lee, H.M. 1989, ApJ, 337, 84
- Hills, J.G., 1975, Nature 254, 295
- Kochanek, C. 1994, ApJ, 422, 508
- Livio, M. & Spruit, H. C. 1991, A&A, 252, 189
- Loska, z., 1981, Acta Astron., 32, 12
- Narayan, R. 1996, “Advective Disks”, to appear in Proc. IAU Colloq. 163 on Accretion Phenomena & Related Outflows, A.S.P. Conf. Series, eds. D. T. Wickramasinghe, L. Ferrario, G. V. Bicknell, astro-ph/9611113
- Narayan, R. & Yi, I. 1995, ApJ, 452, 710
- Nityananda, R. & Narayan, R. 1982, MNRAS, 201, 697
- Paczyński, B. and Sienkiewicz, R., 1972, 22, 73
- Paczyński, B., and Wiita, P. (PW) 1980, A&A, 88, 23
- Phinney, E.S. 1989, in IAU Symposium 136, The Galactic Center, ed. M. Morris (Dordrecht: Kluwer)
- Pringle, J. E. 1974, Ph.D. Thesis, University of Cambridge
- Rees, M. 1988, Nature, 333, 523
- Rybcki, G. B. & Lightman, A. P. 1979, Radiative Processes in Astrophysics (New York: Wiley), Chpt 7.

Smak, J 1984, *Acta Astron* 34, 161

Tassoul, J. 1992, *ApJ*, 389, 375

Ulmer, A. (U97) 1997, *ApJ* (submitted), preprint astro-ph/9706247

Young, P.J., Shields, G.A., Wheeler, J.C. 1977, *ApJ* 212, 367



Table 1:  $M_{\text{BH}} = 10^6$ . Thick disk simulations with (1) the pericenter,  $R_p$ , in units of the tidal radius,  $R_t$ , (2) the total time the thick disk was evolved, in seconds, (3) residual mass after thick disk phase as a fraction of the initial mass of  $0.5 M_\odot$ , (4) the efficiency of accretion (eq. 27), (5) the time,  $t_1$ , for a thin disk with 6% accretion efficiency to reach  $L_{\text{bol}}/M_{\text{BH}} = L_\odot/M_\odot$  assuming self-similar evolution discussed in § 7, (6) the time,  $t_{\text{adv}}$ , at which the thin disk could shift to an advection dominated mode if  $\alpha \sim 0.1$ , (7) the time,  $t_2$ , for a thin disk which is advection dominated with  $\alpha \sim 0.1$  to reach  $L_{\text{bol}}/M_{\text{BH}} = L_\odot/M_\odot$ . Runs labeled “a” have a restricted viscosity parameter,  $\alpha$  (generally  $\lesssim 10^2$ ), such that the disk does not accrete faster than the debris can circularize. Runs labeled “b” allow for the outer disk to cool and become thin as described in § 4.3 and allow the maximum viscosity. Runs labeled “c” allow the the maximum viscosity ( $\alpha = 1$  and therefore the least efficient accretion. In runs labeled “d,” the disks cooled and became thin before any accretion took place.

$R_p(R_t)$	$t_{\text{tot}}$	$m_{\text{res}}$	effic	$t_1$	$t_{\text{adv}}$	$t_2$	notes
2				$3.0 \times 10^4$	$2.4 \times 10^2$	$2.4 \times 10^3$	a,d
2	$3.5 \times 10^6$	0.42	0.012	$2.8 \times 10^4$	$2.2 \times 10^2$	$2.2 \times 10^3$	b
2	$9.6 \times 10^6$	0.18	0.019	$2.6 \times 10^4$	$2.0 \times 10^2$	$2.0 \times 10^3$	c
1	$1.6 \times 10^7$	0.52	0.033	$2.3 \times 10^4$	$1.8 \times 10^2$	$1.8 \times 10^3$	a
1	$2.9 \times 10^6$	0.34	0.0083	$1.9 \times 10^4$	$1.6 \times 10^2$	$1.6 \times 10^3$	b
1	$7.1 \times 10^6$	0.12	0.014	$1.8 \times 10^4$	$1.4 \times 10^2$	$1.4 \times 10^3$	c
0.5	$9.7 \times 10^6$	0.26	0.016	$1.5 \times 10^4$	$1.2 \times 10^2$	$1.2 \times 10^3$	a
0.5	$3.0 \times 10^6$	0.22	0.0063	$1.3 \times 10^4$	$1.0 \times 10^2$	$1.0 \times 10^3$	b
0.5	$6.0 \times 10^6$	0.08	0.01	$1.2 \times 10^4$	$9.4 \times 10^1$	$9.4 \times 10^2$	c

Table 2:  $M_{\text{BH}} = 10^{6.5}$ . For description, see table 1.

$R_p(R_t)$	$t_{\text{tot}}$	$m_{\text{res}}$	effic	$t_1$	$t_{\text{adv}}$	$t_2$	notes
2				$1.4 \times 10^4$	$1.1 \times 10^2$	$1.1 \times 10^3$	a,d
2	$2.0 \times 10^6$	0.35	0.015	$1.2 \times 10^4$	$9.8 \times 10^1$	$9.8 \times 10^2$	b
2	$1.6 \times 10^5$	0.20	0.015	$1.1 \times 10^4$	$8.5 \times 10^1$	$8.5 \times 10^2$	c
1	$8.5 \times 10^6$	0.56	0.037	$9.1 \times 10^3$	$7.3 \times 10^1$	$7.3 \times 10^2$	a
1	$1.5 \times 10^6$	0.25	0.0093	$7.8 \times 10^3$	$6.3 \times 10^1$	$6.3 \times 10^2$	b
1	$2.6 \times 10^6$	0.13	0.013	$7.0 \times 10^3$	$5.6 \times 10^1$	$5.6 \times 10^2$	c
0.5	$3.3 \times 10^6$	0.21	0.011	$4.6 \times 10^3$	$3.7 \times 10^1$	$3.7 \times 10^2$	a
0.5	$1.0 \times 10^6$	0.11	0.0048	$4.1 \times 10^3$	$3.3 \times 10^1$	$3.3 \times 10^2$	b
0.5	$1.4 \times 10^6$	0.08	0.0068	$4.3 \times 10^3$	$3.5 \times 10^1$	$3.5 \times 10^2$	c

Table 3:  $M_{\text{BH}} = 10^7$ . For description, see table 1.

$R_p(R_t)$	$t_{\text{tot}}$	$m_{\text{res}}$	effic	$t_1$	$t_{\text{adv}}$	$t_2$	notes
2				$6.7 \times 10^4$	$5.4 \times 10^1$	$5.3 \times 10^2$	a,d
2	$1.0 \times 10^6$	0.25	0.015	$4.6 \times 10^4$	$3.7 \times 10^1$	$3.7 \times 10^2$	b
2	$1.1 \times 10^6$	0.21	0.016	$4.5 \times 10^4$	$3.6 \times 10^1$	$3.6 \times 10^2$	c
1	$5.3 \times 10^6$	0.64	0.056	$4.3 \times 10^4$	$3.5 \times 10^1$	$3.5 \times 10^2$	
1	$5.5 \times 10^5$	0.11	0.0060	$2.3 \times 10^4$	$1.9 \times 10^1$	$1.9 \times 10^2$	b
1	$5.6 \times 10^5$	0.10	0.0061	$2.3 \times 10^4$	$1.8 \times 10^1$	$1.8 \times 10^2$	c
0.5	$5.5 \times 10^5$	0.05	0.0024	$5.8 \times 10^3$	$4.7 \times 10^0$	$4.7 \times 10^1$	
0.5	$2.9 \times 10^4$	0.01	0.00045	$3.0 \times 10^3$	$2.4 \times 10^0$	$2.4 \times 10^1$	b
0.5	$5.9 \times 10^5$	0.01	0.00038	$2.6 \times 10^3$	$2.1 \times 10^0$	$2.1 \times 10^1$	c

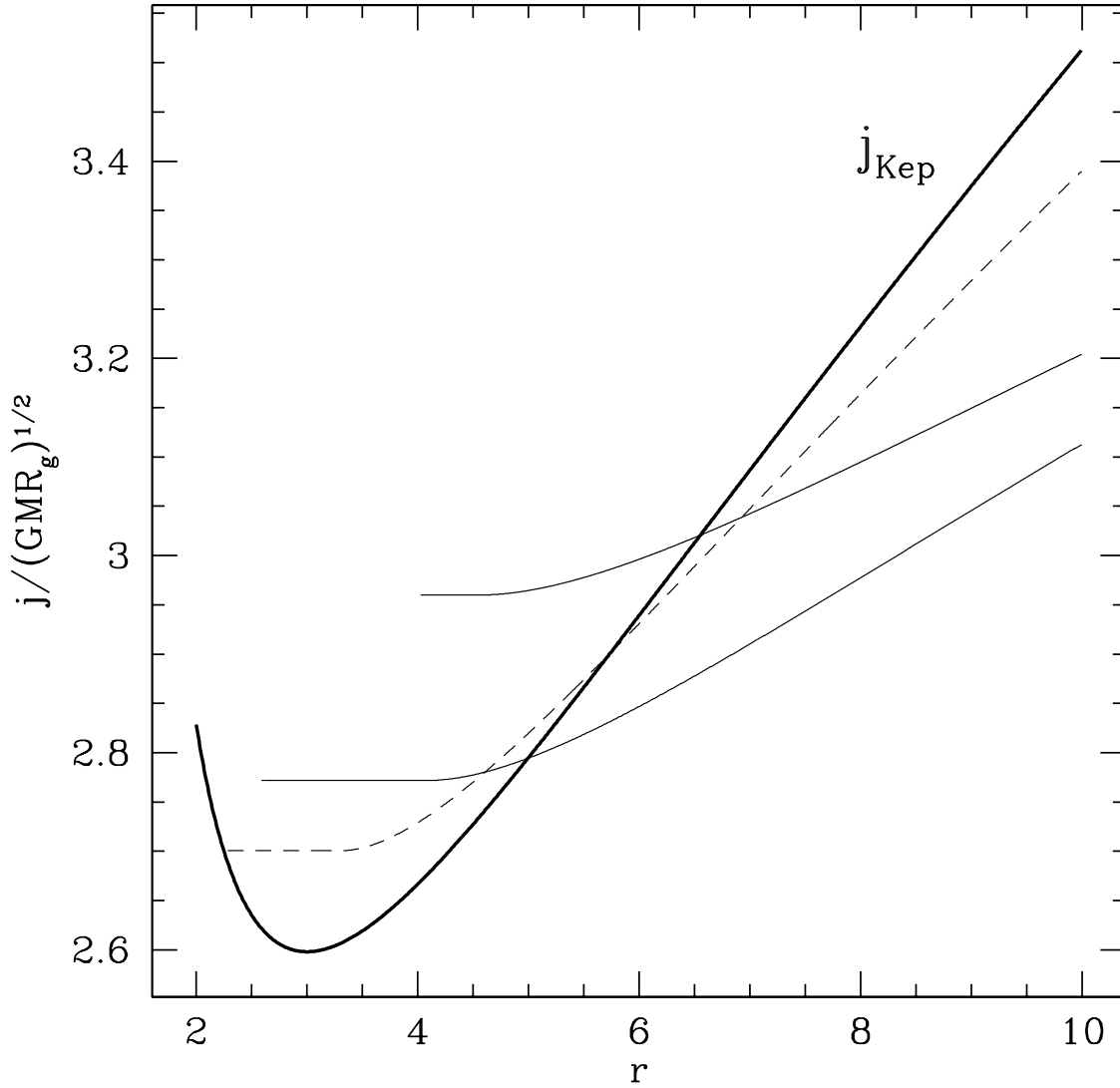


Fig. 1.— Angular momentum as a function of radius for a Keplerian disk (thick solid line; eq. 4) in the pseudo-Newtonian potential of PW, (eq. 3) for non-accreting disks (thin solid lines), and for an accreting disk (dashed line).

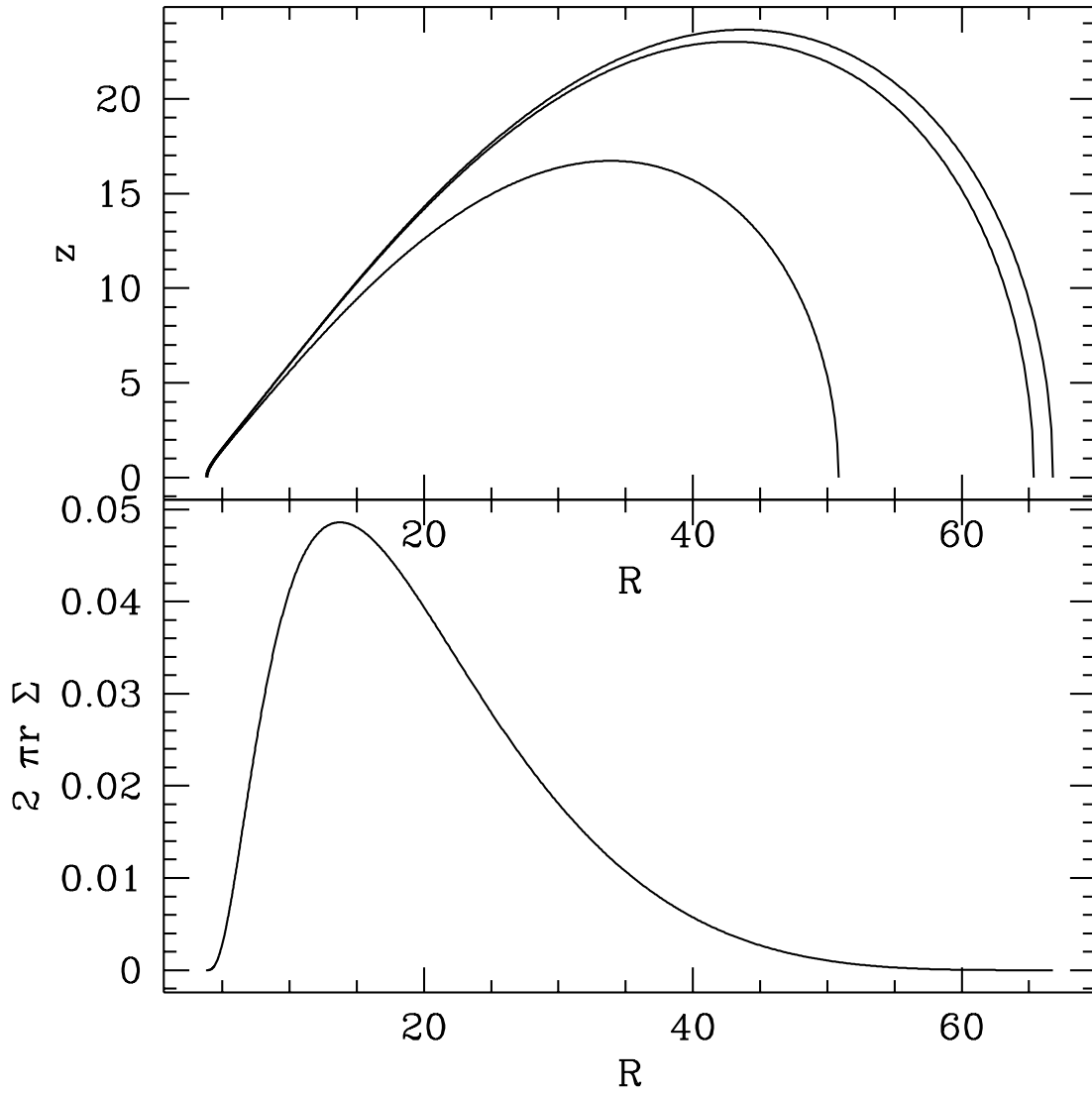


Fig. 2.— A non-accreting thick disk. The top panel shows equipotentials containing 100 % (surface), 95 %, and 50 % of the mass in the  $r/z$  plane. The bottom panel shows the mass distribution as a function of radius.

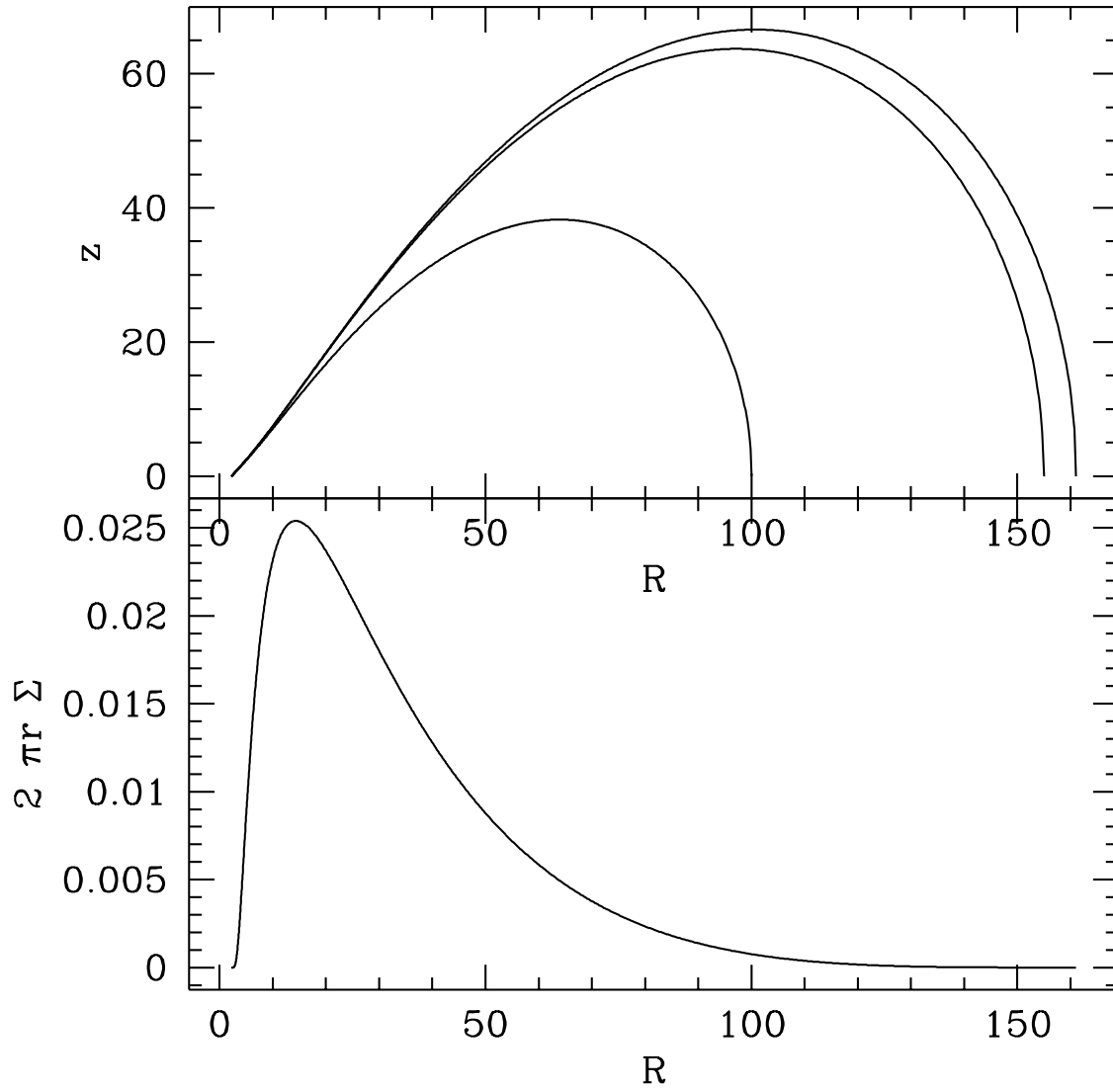


Fig. 3.— An accreting thick disk. The top panel shows equipotentials containing 100 % (surface), 95 %, and 50 % of the mass in the  $r/z$  plane. The bottom panel shows the mass distribution as a function of radius.

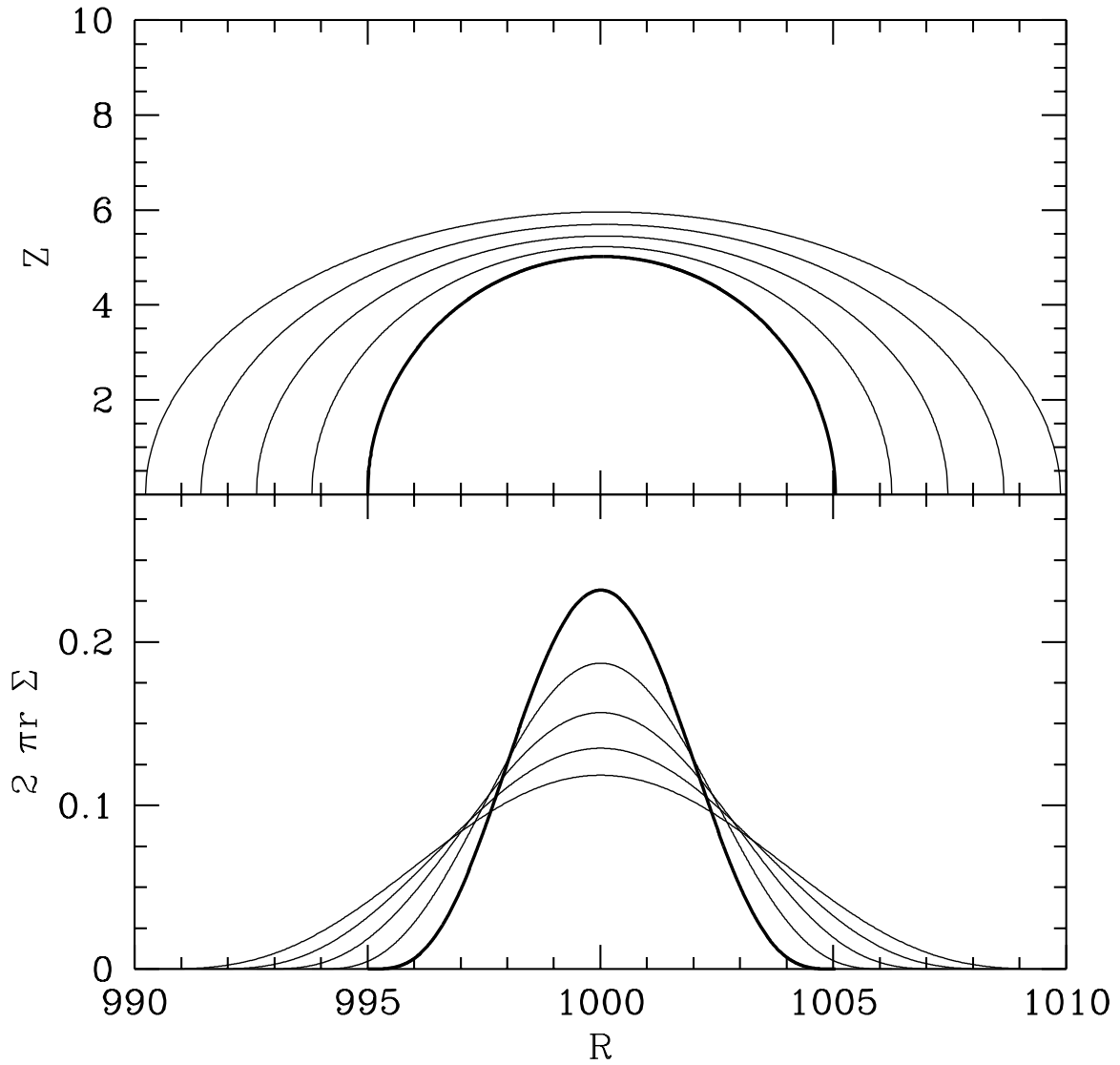


Fig. 4.— Evolution of a circular tube into a disk using the evolution code. The code well reproduces the analytical results of Appendix B. The top panel shows cross-sections of the surface at different times. The bottom panel shows the mass distribution as a function of radius.

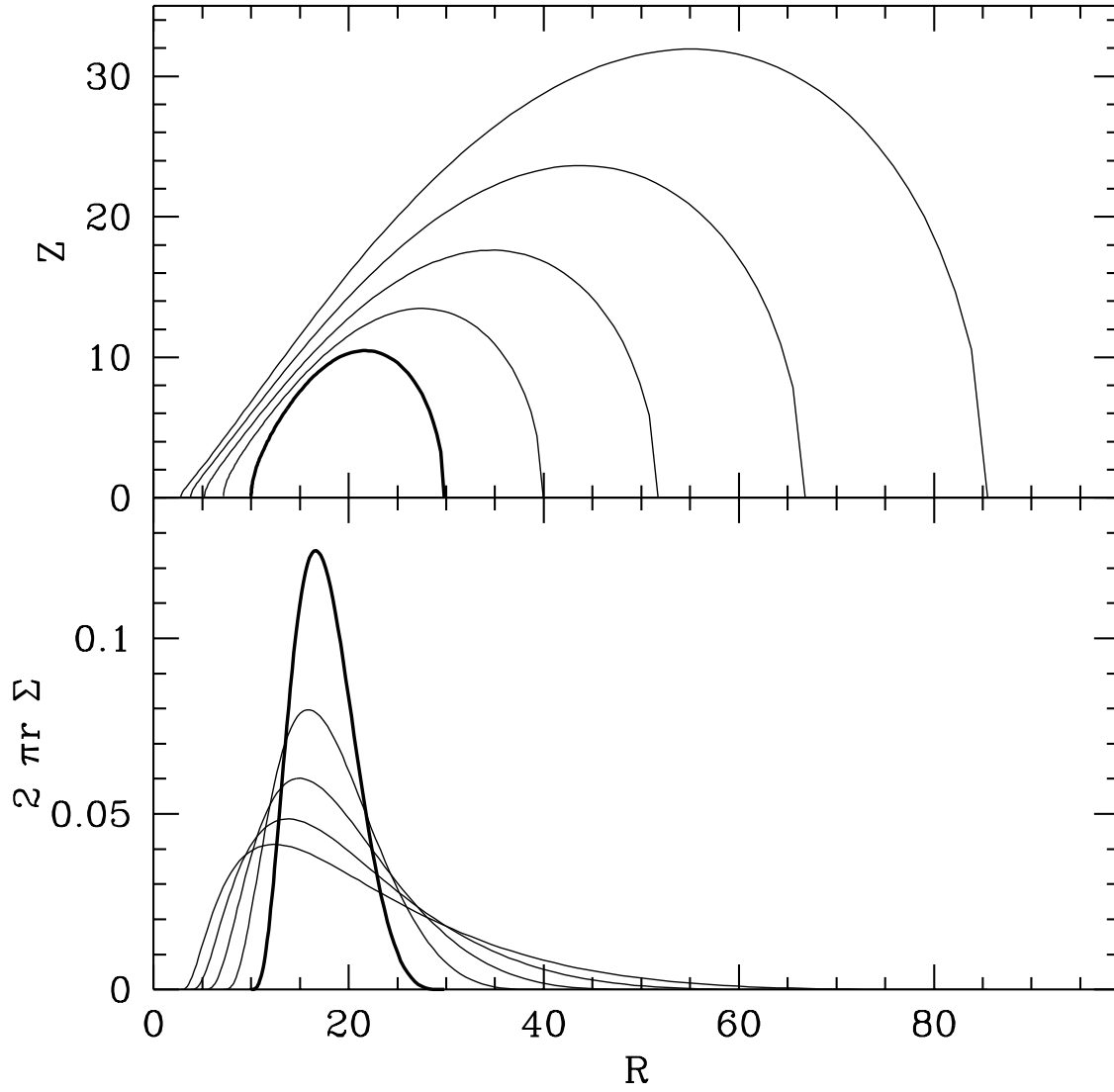


Fig. 5.— Evolution of a non-accreting disk in the limit that very little energy is radiated. The initial model is shown as a thicker line. The different curves correspond to the disk at different times as it expands.

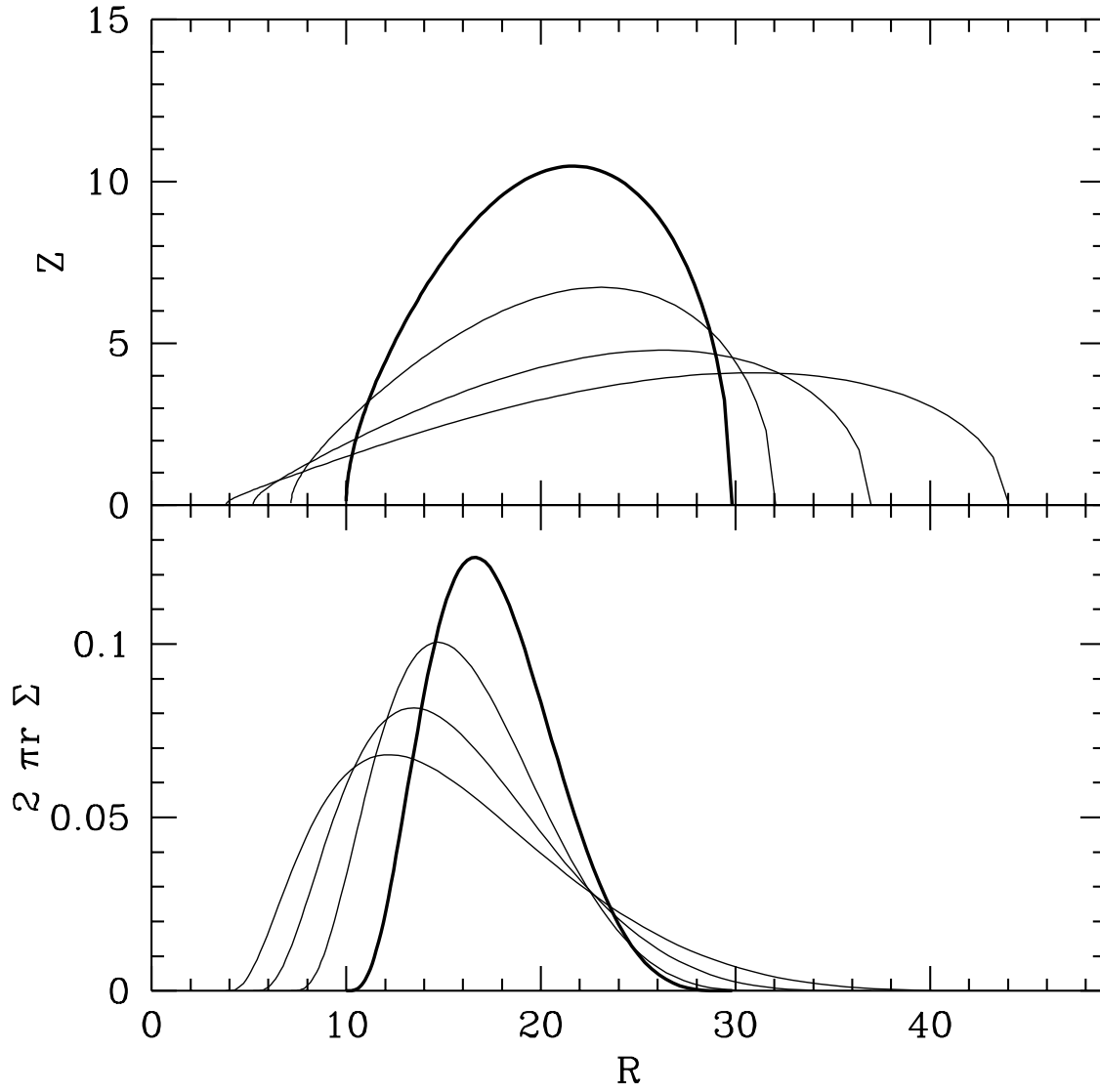


Fig. 6.— Evolution of a non-accreting disk in the limit that the maximum energy is radiated at each step, so that the disk quickly becomes thin. The initial model is shown as a thicker line. The different curves correspond to the disk at different times as it expands.